Polyelectrolyte Diblock Copolymer Micelles

Small Angle Scattering Estimates of the Charge Ordering in the Coronal Layer

Johan R. C. van der Maarel

National University of Singapore, Department of Physics, 2 Science Drive 3,
Singapore, 117542

1 Introduction

Amphiphilic diblock copolymers with a polyelectrolyte block comprise two linearly attached moieties: a charged and a hydrophobic chain part. Owing to their specific properties and the increased need of water supported polymer materials, these copolymers have found widespread applications from the stabilization of colloidal suspensions, through encapsulation and delivery of bioactive agents, to the control of gelation, lubrication, and flow behavior [1,2]. Besides these technological applications, progress in this area also has implications for biophysics. Polyelectrolyte brushes are a model system for the external envelope of certain microorganisms (glycocalix) and are thought to play a role in, e.g., cell recognition and cushioning properties of synovial fluid [3, 4]. The hydrophobic attachment provides a mechanism for self-assembling of the copolymers into units of mesoscopic size, which are large compared to the molecular dimensions. Major factors controlling the self-assembled structures are solvent composition, charge, ionic strength, and chemical nature and the respective sizes of the blocks. For ionic diblocks of poly(styrene-*block*-acrylate) (PS-*b*-PA) with a polyelectrolyte (PA) block length smaller than the length of the polystyrene (PS) block, a multitude of different "crew-cut" structures has been observed by Eisenberg and coworkers [5–7]. These structures include hexagonal wormlike cylinders, lamellae, and (compound) vesicles (see Fig. 1). If the length of the core-forming block is comparable to or smaller than the length of the corona-forming block, it was observed that the copolymers associate to form spherical micelles with a hydrophobic core and a polyelectrolyte corona (Fig. 2). It should be noticed, however, that due to the high glass temperature (363 K) of the PS-block, the observed structures are in a frozen meta-stable state and they depend critically on how the samples are prepared. Once the structures are formed after cooling below the glass temperature, the functionality (i.e., aggregation number) and morphology are fixed. We can use this phenomenon however to our advantage, because the frozen structures provide excellent model systems to investigate the properties of the interfacial polyelectrolyte brush without complications related to copolymer rearrangements and concomitant changes in morphology.

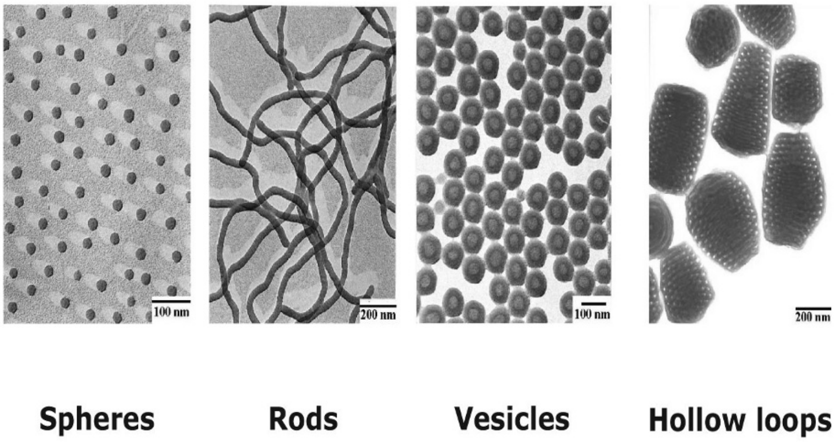

Fig. 1. Asymmetric amphiphilic block copolymers in solution. Transmission electron micrographs reprinted from [7].

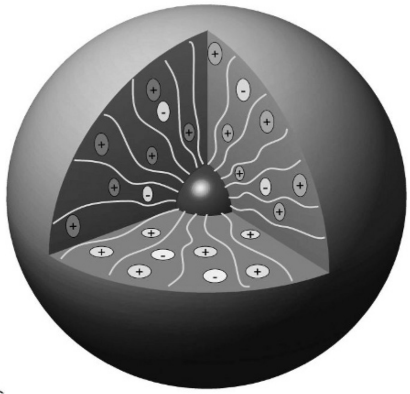

Fig. 2. A schematic drawing of a polyelectrolyte copolymer micelle. The polyelectrolyte corona surrounds the hydrophobic core. The ions are trapped in the coronal layer.

Here, we review our studies of spherical micelles of PS-*b*-PA polyelectrolyte diblock copolymers with degree of polymerization 20 and 85 of the PS and PA blocks, respectively. At ambient temperature, the PS core is in a glassy state, which results in micelles with fixed core size and functionality (the glass temperature of PS, $T_g = 363$ K). The PA corona charge is pH dependent and we will first show with infrared (IR) spectroscopy that the corona charge can be varied between almost zero and full (100%) charge where every monomer carries an ionized group. Transmission electron microscopy (TEM) will be used to verify the micelle morphology. Then we will move on to the investigation of the core and corona size and its relation to charge, screening, and counterion distribution with small angle neutron and X-ray scattering techniques (SANS and SAXS). The main results of these scattering studies are osmotic star-branched polyelectrolyte behavior, full corona chain stretching at high charge and minimal screening conditions, and robustness of the coronal layer against the salinity generated by the addition of salt [8–10]. This behavior is strikingly different from the situation for uncharged spherical polymer brushes and/or star-branched polymers, where the chains take a compact, coiled conformation [11–15]. At low degrees of ionization, the corona charges migrate to the outer micelle region due to the recombination/dissociation balance of the weak polyacid (charge annealing) [16]. We will show that the radial density profile of the counterions is very close to the one for the corona forming copolymer segments and that most, if not all counterions are adsorbed in the coronal layer [17,18]. We will also review SANS and SAXS experiments on our model system up to concentrations where the coronas have to shrink and/or interpenetrate in order to accommodate the micelles in the increasingly crowded volume [19,20]. In the latter studies, it is observed that, irrespective of ionic strength, the corona shrinks with increasing packing fraction. At high charge and minimal screening conditions, the corona layers eventually interpenetrate once the volume fraction exceeds a certain critical value. Finally, we will show that this interpenetration of the arms of the micelle has a profound effect on the fluid rheology.

2 Small Angle Neutron and X-Ray Scattering

From intensities to structure factors. The structure factors describing the density correlations of the PS and PA copolymer blocks are obtained with SANS and contrast matching in water by variation of the H_2O/D_2O solvent composition. We will also review SANS experiments in which the structural arrangement of tetramethylammonium (TMA^+) counterions in the coronal layer of PS-*b*-PA micelles (PS-*b*-TMAPA) is investigated. The use of TMA^+ counterions instead of Na^+ allows contrast variation by isotope labeling of the counterion. For this purpose, a fraction of the TMA counterions is labeled by deuteration, while the contributions to the scattering related to the PA-blocks are blanked by contrast matching in water. In the case of our SAXS experiments, we have neutralized the polyelectrolyte copolymer with CsOH. Since the Cs^+ ion is much heavier (atomic number $Z = 55$) than the organic copolymer atoms, the scattering is dominated by the counterions in the coronal layer. Accordingly, the SAXS intensity is directly proportional to the counterion structure factor, but there is also a small contribution from the copolymer.

For a diblock PS(N_{PS})-*b*-PA(N_{PA}) copolymer solution, with N_{PS} and N_{PA} the number of monomers of the PS and PA block, respectively, it is convenient to consider the blocks as the elementary scattering units [21]. Every PS block is attached to a PA block, and, hence, the macroscopic block concentrations exactly match the copolymer concentration $\rho_{PS} = \rho_{PA} = \rho$. The coherent part of the solvent corrected scattering intensity is given by

$$I(q)/\rho = \sum_{i,j} \bar{b}_i \bar{b}_j N_i N_j \, S_{ij}(q) \tag{1}$$

where the summation runs over all structure factors $S_{ij}(q)$ pertaining to the density correlations among the solutes ($i = j =$ PS, PA, and TMA; S_{ii} is abbreviated as S_i) and solute pairs ($i \neq j$). The scattering length contrast reads $\bar{b}_i = b_i - b_s \bar{v}_i / \bar{v}_s$, where the solute ($i$) and solvent ($s$) have scattering lengths b_i and b_s and partial molar volumes $\bar{v}_i$ and $\bar{v}_s$, respectively. Here, the contrast is matched either in water by variation of b_s through the H_2O/D_2O solvent composition (PS and PA) or by variation of b_i through deuteration of the counterion (TMA). Momentum transfer q is defined by the wavelength λ and scattering angle θ between the incident and scattered beam according to $q = 4\pi/\lambda \sin(\theta/2)$. The partial structure factors $S_{ij}(q)$ are the spatial Fourier transforms of the density correlation functions

$$S_{ij}(q) = \rho^{-1} \int_V d\boldsymbol{r} \exp(-i\boldsymbol{q} \cdot \boldsymbol{r}) \langle \rho_i(0) \rho_j(\boldsymbol{r}) \rangle \tag{2}$$

In a selective solvent, the copolymers form spherical aggregates with a hydrophobic PS block core and a polyelectrolyte PA block corona. If the radial density of the corona is assumed to be invariant to fluctuations in inter-micelle separation, the structure factor Eq. (2) takes the form

$$S_{ij}(q) = N_{ag}^{-1} F_i(q) F_j(q) \;\; S_{cm}(q) \tag{3}$$

with the micelle aggregation number N_{ag}, the form factor amplitude $F_i(q)$, and the micelle center of mass structure factor $S_{cm}(q)$. In the absence of interactions between the micelles and/or at sufficiently high values of momentum transfer $S_{cm}(q)$ reduces to unity. The form factor amplitude $F_i(q)$ can be expressed in terms of the *radial* core ($i =$ PS) or corona ($i =$ PA) density $\rho_i(r)$

$$F_i(q) = \int_{V_{micelle}} d\boldsymbol{r} \exp(-i\boldsymbol{q} \cdot \boldsymbol{r}) \, \rho_i(\boldsymbol{r}) = \int dr \sin(qr)/(qr) 4\pi r^2 \rho_i(r) \tag{4}$$

The scattering amplitudes are normalized to N_{ag} at $q = 0$.

Solution structure factor. For polyelectrolyte copolymer micelles, an analytic expression for the center of mass solution structure factor is not available. We have analyzed the data with a hard sphere potential and the Percus-Yevick approximation for the closure relation [22]. The solution structure factor has the form

$$S_{cm}^{-1}(q) - 1 = 24\phi \left[\alpha f_1 \left(D_{hs} q\right) + \beta f_2 \left(D_{hs} q\right) + \phi\alpha f_3 \left(D_{hs} q\right)/2\right] \tag{5}$$

with

$$\alpha = \frac{\left(1+2\phi\right)^2}{\left(1-\phi\right)^4} \quad , \quad \beta = -\frac{3\phi\left(2+\phi\right)^2}{2\left(1-\phi\right)^4} \tag{6}$$

and

$$\begin{aligned} f_1(x) &= \left(\sin(x) - x\cos(x)\right)/x^3 \\ f_2(x) &= \left(2x\sin(x) - (x^2-2)\cos(x) - 2\right)/x^4 \\ f_3(x) &= \left((4x^3 - 24x)\sin(x) - (x^4 - 12x^2 + 24)\cos(x) + 24\right)/x^6 \end{aligned} \tag{7}$$

The fit parameters are the hard sphere diameter D_{hs} and the volume fraction $\phi = \pi/6 D_{hs}^3 \rho_{mic}$ with micelle density ρ_{mic}. The hard sphere diameter should be interpreted as an effective diameter; its value could be smaller than the outer micelle diameter if interpenetration occurs. Furthermore, it is known that for soft objects the hard sphere potential does not correctly predict the relative amplitudes of the primary and higher order correlation peaks [23]. As will be discussed below, we have also tested a sticky hard sphere model and a repulsive screened Coulomb potential [24, 25]. However, the effect of electrostatic interaction among the micelles was found to be modest, which is attributed to the fact that almost all neutralizing counterions are confined in the coronal layer.

Core and corona form factors. The core can be described by a homogeneous dense sphere with density ρ_{PS} and diameter D_{core}. Accordingly, the radial PS block density is uniform for $0 \leq 2r \leq D_{core}$ and given by $\rho_{PS}(r)\pi D_{core}^3/6 = N_{ag}$ and zero for $2r > D_{core}$. For such uniform profile, the core scattering amplitude reads

$$F_{PS}(q) = N_{ag} 3 \left(\sin\left(qD_{core}/2\right) - \left(qD_{core}/2\right)\cos\left(qD_{core}/2\right)\right)/\left(qD_{core}/2\right)^3 \tag{8}$$

Due to the relatively small core size and the mutual segment repulsion induced by the charge, the density in the coronal layer is non-uniform and varies along with the radius away from the core. To describe the corona structure we will adopt an algebraic radial PA block density profile

$$\rho_{PA}(r) = \rho_{PA}^0 \ \left(2r/D_{core}\right)^{-\alpha} , \ \ D_{core} < 2r < D_{mic} \tag{9}$$

where corona chain statistics determines the value of α and ρ_{PA}^0 is the density at the core - corona interface. The latter interfacial density is related to the outer micelle diameter D_{mic} through the normalization requirement (i.e., by integration of the radial profile)

$$\pi\left(D_{mic}^{3-\alpha}D_{core}^{\alpha}-D_{core}^{3}\right)=2\,(3-\alpha)\,N_{ag} \tag{10}$$

We will calculate the corona form factor amplitude with algebraic profile (9) by numeric integration, although analytical expressions are available [26]. The core PS and corona PA form factors are related to the square of the scattering amplitudes and take the form

$$P_{PS}(q)=F_{PS}^{2}(q)/N_{ag}\ ,\ P_{PA}(q)=F_{PA}^{2}(q)/N_{ag} \tag{11}$$

The algebraic profile (9) accounts for the *average* corona density scaling and neglects corona chain *fluctuations.* The effect of fluctuations on the scattering behavior is important when the momentum transfer is on the order of the intermolecular correlation distance within the corona. Furthermore, they contribute to the corona structure factor ($= S_{PA}$) only, the cross term S_{PA-PS} is unaffected due to the heterodyne interference between the amplitudes scattered by the homogeneous core and heterogeneous corona [27,28].

3 Corona Chain Statistics

The value of the density scaling exponent α is determined by the chain statistics in the coronal layer. We will gauge the corona statistics from the scaling approaches for star-branched polymers. These polymers can also serve as a model for spherical diblock copolymer micelles. The fact that the coronal region cannot extend right to the center of the micelle merely sets a certain minimum correlation length (i.e., blob size) at the core-corona interface. In the scaling approach the blob size ξ is determined by the condition that the chain remains unperturbed within the blob [29,30]. Each blob contains g monomers, each monomer with a step length l. The blob size ξ is related to the number of monomers g according to

$$\xi \simeq l g^{\nu} \tag{12}$$

where the value of ν is determined by the chain statistics inside the blob, e.g. $\nu = 1/2$ if the chain is Gaussian and $\nu = 3/5$ with chain excluded volume interactions. For a star-branched spherical micelle, both g and ξ may vary along the radius r away from the core. The radial corona density scales as the number of monomers $N_{ag}g\,(r)$ in the shell of radius r and thickness $\xi(r)$

$$\rho_{PA}(r) \simeq N_{ag}g(r)/\left(r^{2}\xi(r)\right) \tag{13}$$

and the exponent α in (9) can be derived from (12) and (13), together with a certain radial dependence of the blob size $\xi(r)$.

In the case of a neutral star-branched micelle, close packing of the blobs in the shell of radius r implies the radial dependence of the blob size $\xi(r) \simeq N_{ag}^{-1/2}r$. In this Daoud–Cotton expanding blob model, the density scaling takes hence the form $\rho_{PA}(r) \simeq l^{-1/\nu}N_{ag}^{(3\nu-1)/(2\nu)}r^{(1-3\nu)/\nu}$ and $\alpha = 1$

or 4/3 without ($\nu = 1/2$) or with ($\nu = 3/5$) excluded volume interactions, respectively [11]. Borisov and Zhulina have derived scaling expressions for the size and radial density distribution of star-branched polyelectrolytes with and without screening by added salt [31, 32]. Furthermore, due to the recombination and dissociation balance of the weak polyacid block, migration of charges toward the outer coronal region (charge annealing effects) might be important. Here, we will summarize the scaling results for polyelectrolyte stars, as far as they are relevant for the interpretation of the scattering data. For a derivation of the pertinent equations, the reader is referred to the papers by Borisov and Zhulina [31, 32].

Without the presence of supporting electrolyte, two different classes of star-branched polyelectrolytes exist. When the fraction f_q of ionized groups is very small, the electrostatic screening length is much larger than the micelle size and, hence, inside the corona there is no screening of Coulomb interaction. With increasing f_q the majority of the counterions are trapped within the corona and, now, the concomitant osmotic pressure gives the main contribution to the corona stretching force. The transition between the unscreened and the screened, osmotic, micelle occurs at a critical charge fraction

$$f_q^* \simeq (l/l_B)^{1/\nu} N_{ag}^{-1/\nu} \tag{14}$$

with l_B the Bjerrum length (0.7 nm at 298 K). For micelles with a large aggregation number, the unscreened regime can only be observed if $f_q \ll 1$. Due to the large aggregation number (around 100), most, if not all, of our samples are in the osmotic regime, and, accordingly, we will only summarize the results for osmotic micelles. As a surprising result, the outer diameter of the osmotic micelle does not depend on the aggregation number and scales with the corona charge fraction according to

$$D_{mic} \simeq N l f_q^{1-\nu} \tag{15}$$

The radial scaling of the blob size $\xi(r)$ can be derived from the balance of the elastic, conformational, stretching force and the osmotic pressure exerted by the counterions trapped inside the blob. Since the fraction of trapped counterions does not vary along the radius, the blob size in the outer region of the corona is constant and is given by

$$\xi \simeq l\, f_q^{-\nu} \tag{16}$$

The formation of radial strings of blobs of uniform size and, hence, uniform mass per unit length results in a density scaling

$$\rho_{PA}(r) \simeq N_{ag} l^{-1} f_q^{\nu-1} r^{-2} \tag{17}$$

and hence $\alpha = 2$. Due to space restrictions, in the inner-corona region the blobs are expected to increase in size (with α on the order of unity) with increasing distance away from the core until the critical size given by (16) is reached. The crossover radial distance r^* between the expanding and constant blob size regions is $r* \simeq l\, f_q^{-\nu}$. With increasing f_q, the expanding blob size region shrinks and eventually vanishes if r^* becomes on the order of the core radius $D_{core}/2$. Concurrently, due to the osmotic pressure of the counterions, the corona becomes uniformly extended ($\alpha = 2$) and can be envisioned as strings of blobs of constant size given by (16). The presence of the core limits the range over which the blobs are allowed to expand. This is in contrast to the situation of star-branched polyelectrolytes, where the expanding blob region extends right to the center of the star.

An additional screening of Coulomb interaction becomes important when the concentration ρ_s of added salt exceeds the concentration of counterions ρ_i in the coronal layer. The corona stretching force is now proportional to the difference in osmotic pressure of co- and counterions inside and outside the micelle. This difference in osmotic pressure can be obtained by employing the local electroneutrality condition and Donnan salt partitioning between the micelle and the bulk of the solution. The micelle outer radius is obtained by balancing the total osmotic stretching force with the elastic force. In the salt dominated regime (i.e., if $\rho_s \gg \rho_i$), the overall diameter of the micelle scales as

$$D_{mic} \simeq \left(N_{ag}\, l^2\, f_q^2\, N^3\right)^{1/5}\ \rho_s^{-1/5} \tag{18}$$

An increase in salt concentration results hence in a gradual contraction of the micelle, because of additional screening of the Coulomb repulsion among the ionized polyelectrolyte block monomers (i.e., a decrease in electrostatic excluded volume interactions). The radial dependence of the blob size

$$\xi\,(r) \simeq \left(N_{ag}\, l^4\, f_q^2 \rho_s^{-1}\right)^{-1/3}\ r^{2/3} \tag{19}$$

is obtained from the local balance of differential osmotic force and the local tension in the star arms. As each arm exhibits locally Gaussian statistics ($\xi \simeq l g^{1/2}$), the block density profile can derived from (13) and (19) and reads

$$\rho_{PA}\,(r) \simeq \left(N_{ag}^2 f_q^{-2} \rho_s l^{-2}\right)^{1/3} r^{-4/3} \tag{20}$$

The radial decay of the monomer density is described by the same exponent as in neutral star-branched polymers with excluded volume interactions in a good solvent. Accordingly, in the salt dominated regime ($\rho_s \gg \rho_i$), the corona density scaling exponent takes the Daoud-Cotton expanding blob value $\alpha = 4/3$. However, in contrast to neutral stars, the elastic blobs in partially screened polyelectrolyte micelles have a blob-size scaling exponent 2/3 (19) rather than unity and hence they are not closely packed.

For polyelectrolyte stars at intermediate ionic strengths, Borisov and Zhulina proposed a multiple-region-scaling model. At small distances from the core, where $\rho_i > \rho_s$, the corona statistics is not affected by the added salt. Here, the chains are extended in the radial direction with uniform mass per unit length ($\alpha = 2$, in the innermost coronal region α may be of the order of unity due to space restrictions). With increasing distance away from the core, the local counterion concentration decreases and for $r > r_s$ the screening is governed by the salt. Hence, in the outer corona region, where $\rho_s \gg \rho_i(r)$, the corona density scaling exponent takes the value $\alpha = 4/3$. The crossover distance

$$r_s \simeq \left(N_{ag}\, l^{-1}\, f_q^{\nu}\right)^{1/2} \rho_s^{-1/2} \tag{21}$$

is determined by the equality of the local counterion concentration $\rho_i(r) = f_q \rho_{PA}(r)$ in the coronal layer of the osmotic star [with radial density from (17)] and the salt concentration ρ_s in the bulk. With the addition of simple salt, the fully ionized micelle contracts according to (15) with a concomitant decrease in the crossover distance r_s between the inner- and outer-corona scaling regimes with density scaling exponents $\alpha = 2$ and 4/3, respectively. The salt penetrates the micelles and the radial decay of the monomer density scaling in the outer region is similar to the situation for neutral star-branched polymers. The blobs are not closely packed however and increase in size away from the crossover according to (19). The inner-corona region, characterized by radial strings of blobs of uniform size, remains unaffected until the salt concentration competes with the salinity generated by the counterions coming from the dissociation of the polyelectrolyte.

PA is a weak polyacid and at low fraction of ionized monomers ($f_q \ll 1$) the effects of charge annealing are important. In the simplest approximation, the local charge fraction $f_q(r)$ is determined by the (presumably r-independent) ionization constant K and the mass action law $K = \rho(r) f_q(r)^2 / \left(1 - f_q(r)\right) \approx \rho(r) f_q(r)^2$. Because of the dissociation and recombination balance, the charge fraction is now no longer constant and increases according to $f_q(r) \sim r^{2/(1+\nu)}$. A remarkable result of this charge annealing effect is that the local tension in the branches now increases with increasing distance away from the core. As the branches become more extended with increasing r, the blob size ξ decreases $\xi(r) \simeq l\, r^{-2\nu/(1+\nu)}$ and the monomer density decays faster [32]

$$\rho_{PA}(r) \simeq l^{-1} r^{-4/(1+\nu)} \tag{22}$$

The density scaling exponent α takes the value 8/3 or 5/2 without ($\nu = 1/2$) or with ($\nu = 3/5$) volume interactions, respectively. Although the addition of salt might shift the recombination-dissociation balance and, hence, influence the ionization constant K (by replacing hydronium ions by cations from the salt), the corona scaling behavior is not affected. Furthermore, in our experiments, the added salt concentration is in excess of the counterion concentration and the additional screening results in a contraction of the coronal layer according to $D_{mic} \sim \rho_s^{-1/5}$, as in the case of highly charged micelles. The different scaling regimes under various conditions are illustrated in Fig. 5.

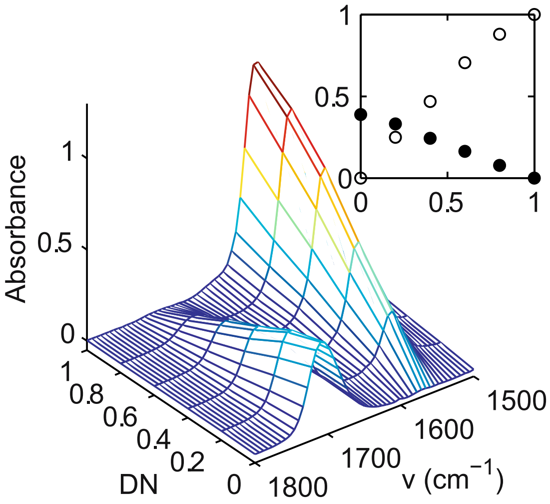

Fig. 3. IR spectra versus degree of neutralization DN from 0.15 mole of PA/dm^3 PS-*b*-PA solutions [16]. The inset displays the integrated peak intensities of the COO$^-$ (1570 cm^{-1}, open symbols) and C=O (1700 cm^{-1}, closed symbols) asymmetric and symmetric stretching bands, respectively, normalized to the COO-band at $DN = 1$.

4 Polyelectrolyte Block Ionization

The ionization of the poly(acrylic acid) block can be monitored with IR spectroscopy [16]. In the range of 1500 to 1800 cm^{-1} two bands can be distinguished. As displayed in Fig. 3, the charge neutralization results in the appearance of the asymmetric COO$^-$ stretching band at 1570 cm^{-1} with a concurrent disappearance of the C=O stretching band around 1700 cm^{-1}. The relative peak intensities are displayed in the inset of Fig. 3. To a good approximation, the peak intensities are proportional to the molar ratio of (added) alkali and polyacid monomer (i.e., the degree of neutralization DN). The COO$^-$ and the C=O peak intensities vanish in the limit of no ($DN = 0$) and full ($DN = 1$) charge neutralization, respectively. For fully neutralized samples, every acid group of the polyelectrolyte block is ionized. Without the addition of alkali ($DN = 0$), the copolymer is still weakly charged due to the auto-dissociation of the COOH group. However, as judged from potentiometry, the degree of auto-dissociation is of the order 10^{-3} and is beyond the accuracy of the IR experiment [33]. Accordingly, the polyelectrolyte block charge fraction f_q can be tuned between almost zero and unity by adjusting the degree of neutralization DN.

5 Association Morphology

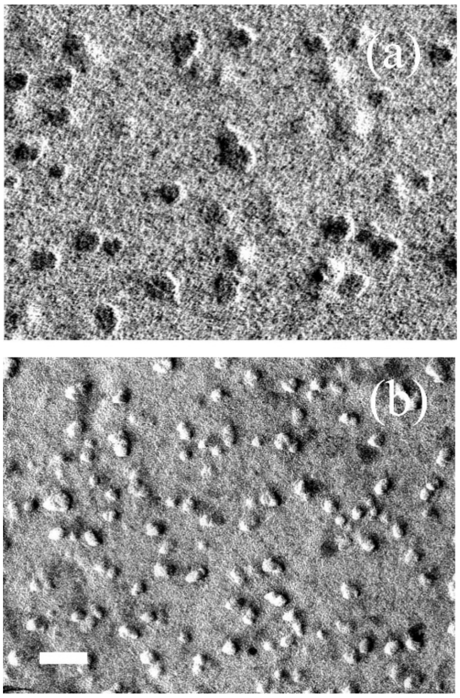

Fig. 4. TEM replicas of PS-*b*-PA solutions with $DN = 1$ (a) and 0 (b) [16]. The $DN = 1$ sample was imaged directly, whereas the $DN = 0$ replica was obtained with freeze-fracture techniques. The bar corresponds to 100 nm. Reproduced from [16]. Copyright (2000) American Chemical Society.

The morphology of the self-assembled structures was examined with TEM [16]. Fig. 4 shows carbon replicas of solutions with full ($DN = 1$) and almost zero ($DN = 0$) polyelectrolyte block charge. The $DN = 1$ sample was imaged directly (after evaporation of the solvent from the grid, film strengthening, and shadowing), whereas the $DN = 0$ replica was obtained with freeze-fracture techniques. For both cases, the replicas show homogeneously dispersed and well separated individual spherical micelles. With the ionization of the polyelectrolyte block, the diameter of the micelles increases due to the concomitant corona expansion from $\sim$30 to $\sim$ 50 nm. The estimated diameters are in the range of those determined by SANS (see below), and the TEM micrographs are, hence, sensitive to the physical extent of the corona. This is not a surprising result, because the carbon/platinum film covers the whole micelle and not only the core (or the freeze-fractured surface). We have nevertheless refrained from further analysis of the TEM micrographs, because of the uncertainties in size estimation introduced by the fracturing and shadowing procedures. The morphology of the individual micelles is further investigated with SANS and contrast matching in the water. As will be shown below, SANS provides an *in situ* measurement technique without the risk of damage and/or micelle deformation caused by the TEM drying or freeze-fracturing procedures.

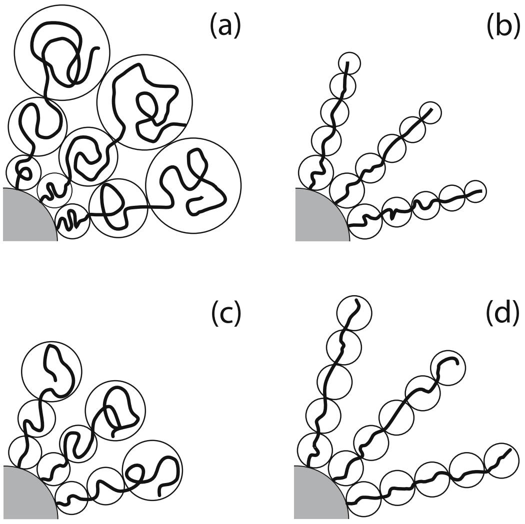

Fig. 5. Schematic representation of the various corona scaling regimes: (a), neutral, space filling expanding blobs with $\rho(r) \sim r^{-4/3}$; (b) weak charge and salt free, radial strings of blobs of decreasing size with $\rho(r) \sim r^{-5/2}$; (c) salt dominated, non space filling radial strings of expanding blobs with $\rho(r) \sim r^{-4/3}$;(d) high charge and salt free, radial strings of blobs of equal size with $\rho(r) \sim r^{-2}$. The scaling laws pertain to locally swollen chains in good solvent.

6 Core Structure

The core PS and corona PA structure factors were determined by SANS and contrast variation in the water. SANS was measured with the D22 and PAXY diffractometers situated on the cold nuclear reactor sources of the Institute Laue-Langevin and Laboratoire Léon Brillouin, respectively. As an illustrative example, the PS partial structure factor pertaining to fully charged micelles without added salt is displayed in Fig. 6 (the corona structure factors will be discussed below) [20]. Here, the copolymer concentration covers the range from the diluted to the concentrated regime where the coronal layers have to shrink and/or interpenetrate in order to accommodate the micelles in the increasingly crowded volume. At the lowest micelle concentration and/or with excess salt, inter-micelle interference is insignificant and the core structure factor can directly be compared with the core form factor. With increasing concentration and minimal screening conditions, a primary and higher order correlation peaks emerge. As is more clearly demonstrated by the SAXS results described below, the position of the primary peak scales with the copolymer concentration ρ according to $\rho^{1/3}$. This scaling behavior is characteristic for micelles with fixed aggregation number and isotropic symmetry in the local environment. There are no changes in the high q behavior of the core structure factor, irrespective charge, the presence of salt, and copolymer concentration. The lines in Fig. 6 represent the model calculations with $D_{core} = 9$ nm (the parameters pertaining to the fit of the center of mass structure factor, D_{hs} and ρ_{mic}, are discussed below). From the absolute normalization of the structure factors in the long wavelength ($q \to 0$), an aggregation number N_{ag} around 100 is derived. The aggregation number agrees with the value obtained from the core size, PS molecular weight, and PS partial molar volume. This shows that the solvent is excluded from the core and the PS is closely packed with a density close to the macroscopic density 1.05 kg/dm^3. The fixed functionality is due to the fact that all experiments were done well below the glass temperature of PS (363 K).

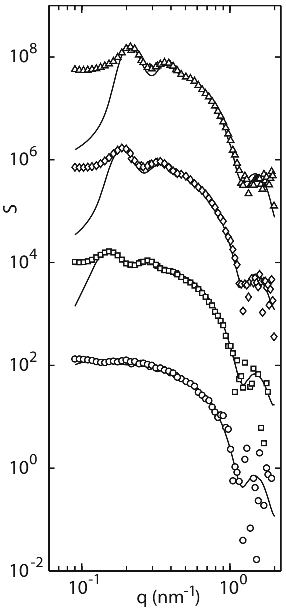

Fig. 6. Core PS structure factor versus momentum transfer for fully charged PS-*b*-PA micelles without added salt [20]. The copolymer concentration is 44 (△), 30 (◇), 17 (□), and 4.4 (○) g/L from top to bottom. The data are shifted along the y-axis with an incremental multiplication factor. The curves represent the model calculations with core diameter 9 nm.

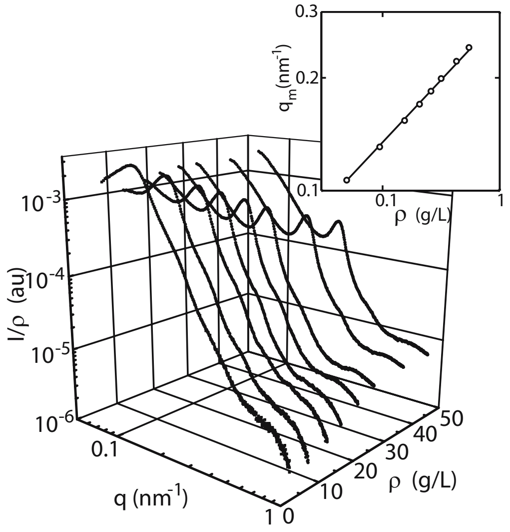

Fig. 7. SAXS intensity divided by copolymer concentration versus momentum transfer for fully charged PS-*b*-CsPA micelles without added salt [20]. The inset shows the peak position q_m versus copolymer concentration ρ in the double logarithmic representation. The line represents $q_m \sim \rho^{1/3}$ scaling.

7 Counterion Structure

The SAXS intensities of the fully neutralized PS-*b*-CsPA micelles divided by copolymer concentration are displayed in Fig. 7 [20]. The synchrotron SAXS experiments were done at the BM26 "DUBBLE" beam line of the European Synchrotron Radiation Facility. Notice that the SAXS intensities are, to a good approximation, proportional to the counterion structure factor, because the scattering is dominated by the heavy Cs^+ ions. As in the case of the core structure factor, the SAXS data show a primary inter-micelle correlation peak. The higher order correlation peaks are less prominent, due to the steep decrease of the counterion structure factor with increasing values of momentum transfer. As seen in the inset of Fig. 7, the position of the primary peak scales with copolymer concentration according to $\rho^{1/3}$. This result confirms the isotropic local structure and fixed aggregation number of the micelles, which has also been observed with SANS. At high values of momentum transfer, the SAXS intensities are seen to increase with increasing concentration. This effect might be due to counterion fluctuations; a fit to a Gaussian background contribution yields a correlation length, which decreases from 1.2 to 0.7 nm with increasing copolymer concentration from 4.5 to 48 g/L, respectively.

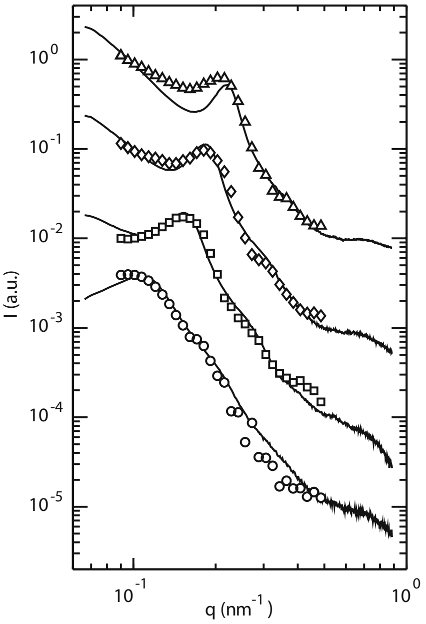

Fig. 8. Comparison of SAXS (solid curves) intensities with the reconstituted SANS intensities (symbols) [20]. The data are shifted along the y-axis with an incremental multiplication factor. The copolymer concentration is 44 (for SAXS 48, △), 30 (◇), 17 (□), and 4.5 (○) g/L from top to bottom. For the most densely concentrated set, notice the slight difference in position of the correlation peak due to a small difference in micelle concentrations. Reprinted with permission from [20]. Copyright (2005) American Institute of Physics.

It is interesting to compare the SAXS data for the PS-*b*-CsPA micelles with the relevant combination of the core PS and corona PA scattering contributions (there is an optimized 2% contribution from PS to the SAXS intensity and this accounts for the scattering of the core). The comparison in Fig. 8 shows a perfect agreement in both the position of the correlation peak and the variation of the structure factor with momentum transfer. We have also measured the counterion structure factor with SANS from 12 g/L samples with isotopically labeled tetramethylammonium (TMA) counterions [17]. The TMA partial structure factor is displayed and compared with the PA (corona) partial structure factor in Fig. 9. The TMA and PA structure factors show an almost perfect match in both the scaling with momentum transfer and absolute normalization. The ratio of the counterion and corona structure factors is, hence, q-independent with an average value 0.99 ± 0.10. The quantitative agreement shows that, within a 10 % error margin, *all* counterions are confined to the coronal region. Furthermore, the distribution of the counterions along the radius is very close to that of the monomers of the corona-forming blocks. It is also clear that the counterions remain strongly correlated with the coronal chains with increasing packing fraction up to and including the regime where the coronal layers interpenetrate. Due to the neutralization of the coronal layer by trapping of the counterions, the micelles are almost electroneutral and the electrostatic contribution to the inter-micelle interaction potential is expected to play a minor role. The concomitant osmotic pressure exerted by the trapped counterions gives, hence, the main contribution to the corona stretching force and the micelles are in the osmotic regime.

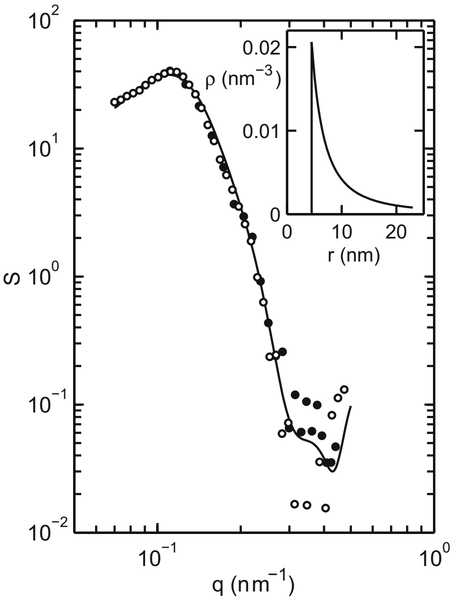

Fig. 9. Comparison of the PA corona and the TMA counterion partial structure factors. (○): PA partial structure factor in PS-*b*-NaPA solutions ($DN = 0.6$). (●): TMA partial structure factor in PS-*b*-TMAPA solutions ($DN = 0.5$) [17]. The polyelectrolyte block concentrations are 0.1 mole of PA/dm^3. The solid curve represents the structure factor with density scaling exponent $\alpha = 2$. The inset displays the radial density. The small difference in the degrees of neutralization (0.6 vs 0.5 for PS-*b*-NaPA and PS-*b*-TMAPA, respectively) has no effect on the corona structure factor beyond experimental accuracy.

8 Corona Structure

From neutral to fully charged micelles. We have measured the PA corona partial structure factors for different degrees of neutralization and at a fixed

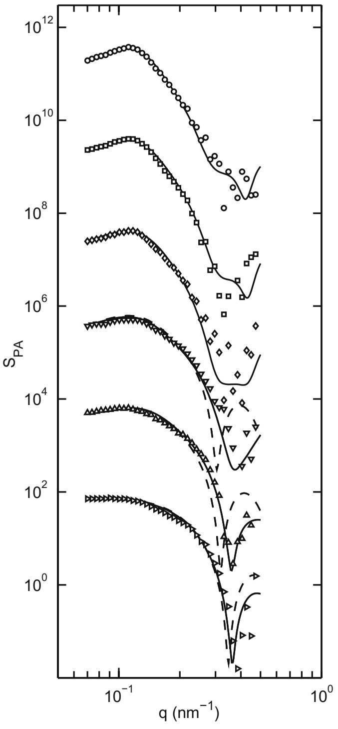

Fig. 10. PA corona partial structure factor versus momentum transfer for salt free micelles with degree of neutralisation: $DN = 1$ (○), 0.6 (□), 0.35 ($\Diamond$), 0.1 ($\bigtriangledown$), 0.04 ($\bigtriangleup$), and 0 ($\cong$) from top to bottom [16]. The data are shifted along the y-axis with an incremental multiplication factor. The copolymer concentration is 12 g/L. The solid curves represent the corona structure factor with corona density scaling exponent $\alpha = 5/2$ for $DN = 0$, 0.04 and 0.1 and $\alpha = 2$ for $DN = 0.35$, 0.6 and 1. The dashed curves represent the corona structure factor with $\alpha = 4/3$ for $DN = 0$, 0.04 and 0.1 only.

micelle concentration (12 g/L) [16]. The results are displayed in Fig. 10. With decreasing degree of neutralization, the corona shrinks and, hence, the structure factor scales toward higher values of momentum transfer and the minimum at $q \approx 0.3$ nm^{-1} becomes more pronounced (in the double logarithmic representation). Furthermore, a correlation peak develops at finite wavelengths, which is similar to the one observed in the core structure factor and is due to the ordering of the micelles. In the case of star-branched polyelectrolytes with a relatively small number of arms ($\sim$ 12), a second correlation peak at higher values of momentum transfer has been reported [34]. The latter peak is due to fluctuations and correlations among the branches within a single star. For the copolymer micelles, the number of branches (i.e., the aggregation number) is much higher around 100. The average segment density within the corona exceeds, say, 0.2 M. As judged from the position of the correlation peak in linear polyelectrolyte solutions at a comparable concentration, the corresponding intra-corona correlation peak is expected at ~ 0.7 nm^{-1} [35]. For such high values of momentum transfer the PA structure factor is very small on the order of the error margin. Hence, the intra-corona correlation peak and the effect of corona chain fluctuations are beyond detection. Furthermore, the copolymer concentration is sufficiently low in the dilute regime that the outer sections of the arms do not overlap (see below). The lines in Fig. 10 are the model structure factors calculated with an average density profile Eq. (9).

Rather than optimizing the density scaling exponent α, the calculation of the corona structure factor was done with $\alpha = 2$ for the samples with degree of neutralization $DN = 0.35$, 0.6 and 1.0. For the weakly charged micelles with $DN = 0$, 0.04 and 0.1, we have plotted the structure factors with $\alpha = 4/3$ and 5/2. The value $\alpha = 2$ is relevant in the case of full stretching of the chains or the formation of radial strings of blobs of uniform size. A density scaling exponent $\alpha = 4/3$ results from the Daoud–Cotton expanding blob model for uncharged star-branched polymers and α takes the value 5/2 in the presence of charge annealing effects. The latter two values refer to good solvent conditions, because water is a good solvent for PA. In the calculation of the corona structure factor, the micelle diameter D_{mic} was optimized, whereas the other parameters were set at their nominal values obtained from the fitting of the PS core structure factor. The fitted diameters versus degree of neutralization to the power 3/5 are displayed in Fig. 11. For highly charged micelles with degree of neutralization 0.35 and higher, an exponent $\alpha = 2$ gives good agreement between the corona structure factor and the data. Although the scaling of the structure factors toward higher q values with decreasing DN can be reproduced by a decrease in outer micelle radius, the results with $\alpha = 2$ fail to describe the position of the minimum at $q \approx 0.4$ nm^{-1} for samples with low corona charge fraction (results not shown). A Daoud–Cotton expanding blob model for neutral stars with $\alpha = 4/3$ shifts the position of the minimum towards too low q values and does not give a good agreement with the data (this is most marked for our $DN = 0.1$ sample). We have checked that an analysis in terms of multiple scaling regimes pertaining to, e.g., expanding and constant blob size regions does not improve the description of the PA structure factor. It is necessary to increase the density scaling exponent α beyond the value two in order to predict the position of the minimum in the structure factor correctly. Indeed, with $\alpha = 5/2$ nice agreement is observed, which shows the importance of the dissociation and recombination balance of the weak polyacid (which results in a migration of the charges towards the outer corona region).

With increasing charge fraction, the micelle diameter first increases, subsequently levels off above 10 % charge neutralization, and reaches the value 25 nm at full charge. The fully stretched value of the radius amounts to 25.5 nm, as estimated from the sum of the core radius 4.5 nm and the contour length

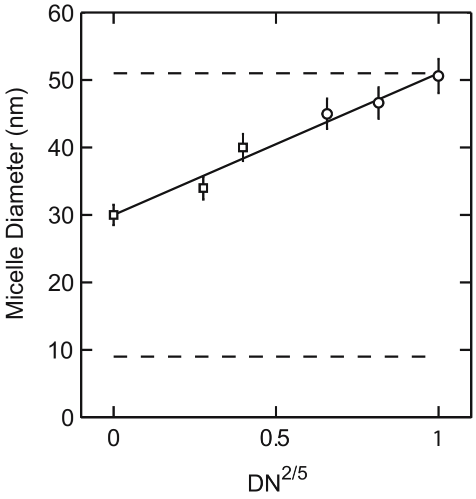

Fig. 11. The micelle diameter versus the scaled degree of neutralization calculated with corona density scaling exponent $\alpha = 2$ (□; $DN = 0.35$, 0.6, and 1) and 5/2 (○ ; $DN = 0$, 0.04, and 0.1) [16]. The bottom and top dashed curves represent the core and fully expanded diameters, respectively. The solid line denotes the scaling result for an osmotic salt-free polyelectrolyte star in a good solvent ($\nu = 3/5$).

of the PA-block (85 monomers per chain with a vinylic step length 0.25 nm). As can be seen in Fig. 11, the NaPA chains in the coronas of the micelles take an almost fully stretched configuration at high pH and no added simple salt. The expansion behavior can be rationalized with the scaling results for star-branched polyelectrolytes in the osmotic regime. According to (14) with $N_{ag} \sim 100$, the transition from the unscreened to the screened, osmotic, micelle occurs at a critical charge fraction $f_q^* \approx 10^{-4}$. Even the non-neutralized ($DN = 0$) micelle carries a sufficient amount of charge to retain the major part of its auto-dissociated protonic counterions inside the corona and, hence, is in the osmotic regime. For osmotic micelles, the micelle radius scales with the charge fraction according to $N\,l\,f_q^{1-\nu}$ (15). To a good approximation, the charge fraction equals the degree of neutralization. Fig. 11 displays the micelle diameter versus the scaled degree of neutralization with the good solvent value $\nu = 3/5$. According to (15) there should be a linear dependence, which is indeed observed within the experimental accuracy.

Salt induced contraction. We will now discuss the response of the corona statistics and micelle diameter to the addition of salt [10]. As in the case of our investigation of the effect of corona charge, the copolymer concentration is fixed at 12 g/L. As can be seen in Fig. 12, with increasing salt concentration the corona shrinks and the structure factor scales toward higher values of momentum transfer with a concurrent sharpening of the minimum at $q \approx 0.3$ nm^{-1} (in the double logarithmic representation). Again, the model structure factors are fitted to the data with an average density profile of the corona given by (9). Without added salt, the fully ionized PA chains are near 100 % stretched with a density scaling exponent $\alpha = 2$ and outer micelle diameter $D_{mic} = 48$ nm. The core and micelle diameter as well as the aggregation number set the PA chain density at the core - corona interface ρ^0_{PA} through the normalization requirement (10) (the grafting density is 2.6^{-1} nm^{-2}). The latter interfacial density was subsequently fixed and the data pertaining to samples with added salt were fitted with Borisov and Zhulina's two-region scaling model [32]. According to this model, the corona is divided into two regions: an inner-corona region where the chain statistics is not affected by the salt ($\alpha = 2$) and an outer region with a density scaling governed by screened electrostatic excluded volume interactions ($\alpha = 4/3$). The crossover distance r_s is the only adjustable parameter and determines, together with ρ^0_{PA}, the outer micelle diameter D_{mic}. The fitted structure factors are also displayed in Fig. 12 and the outer and cross-over diameters, D_{mic} and $2r_s$, respectively are shown in Fig. 13. In particular, the change in shape of the corona structure factor with the addition of salt is nicely reproduced. With the addition of salt, the micelle contracts with a concomitant decrease in r_s. In 1 M excess salt, we almost recover the Daoud–Cotton expanding blob scaling with $\alpha = 4/3$ (the optimized crossover distance between the two different scaling regimes becomes very close to the core radius) and the outer diameter (34 nm) approaches the value pertaining to the pure acid form at minimal screening conditions 30 nm. Accordingly, despite the very high salt concentrations; the range in micelle dimension is similar to the one that can be covered by variation of the corona charge fraction (e.g., by variation of the pH of the supporting buffer medium). The salt-induced contraction can be rationalized with the scaling results for star-branched polyelectrolytes [31,32]. For osmotic micelles in the salt dominated regime, the crossover and the outer micelle diameters scale with the salt concentration according to $\rho_s^{-1/5}$ and $\rho_s^{-1/2}$ [(18) and (21)], respectively. As shown in Fig. 13, these scaling laws are indeed observed within the experimental accuracy. The crossover occurs at an optimized distance r_s, where the concentration of salt ions exceeds that of the corona segments by a factor 0.16, 0.22, and 0.52 in 0.05, 0.2, and 1 M KBr, respectively (note, however, that in 1 M salt the statistics is almost completely governed by the salt). In view of the simplicity of the model (a gradual transition between the two different scaling regions is more likely to occur), this agreement between the counterion and salt concentrations at the crossover distance within an order of magnitude can be considered quite gratifying.

Effects of micelle concentration. We have also measured the corona PA partial structure factor for a range of micelle concentrations from the diluted to the concentrated regime where the coronal layers have to shrink and/or interpenetrate in order to accommodate the micelles in the increasingly crowded volume [19, 20]. The concentration dependence was investigated for samples with degrees of neutralization $DN = 0.1$, 0.5 and 1. Furthermore,

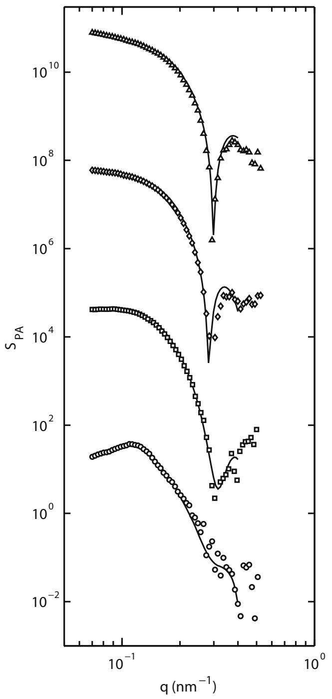

Fig. 12. PA partial structure factor versus momentum transfer for fully ionized micelles ($DN = 1$) with KBr concentrations: $\rho_s = 1$ M (△), 0.2 M (◇), 0.05 M (□), and salt-free (○) from top to bottom [10]. The data are shifted along the y-axis with an incremental multiplication factor. The curves represent the corona structure factor with an inner and outer corona density scaling exponent $\alpha = 2$ and 4/3, respectively, together with the values for the crossover diameters $2r_s$ displayed in Fig. 13.

the micelles were either salt-free or bathed in 0.04 ($DN = 0.1$) and 1 M ($DN = 0.5$ and 1) monovalent salt. As an illustrative example, the results pertaining to fully charged, simple salt free micelles are displayed in Fig. 14. There are no major changes in the high q behavior of the corona structure factor with increasing packing fraction, irrespective charge and ionic strength. This shows that the corona chain statistics is rather insensitive to inter-micelle interaction.

The lines in Figs. 14 represent the model calculations. For salt-free micelles with a charge fraction exceeding 10%, the chains remain almost fully stretched and $\alpha = 2$. For the 10% charged micelles, we have done the model calculations with $\alpha = 5/2$ in accordance with charge annealing towards the outer coronal region due to the recombination-dissociation balance of the weak polyacid. In the presence of excess salt, the corona structure factors are compared with the

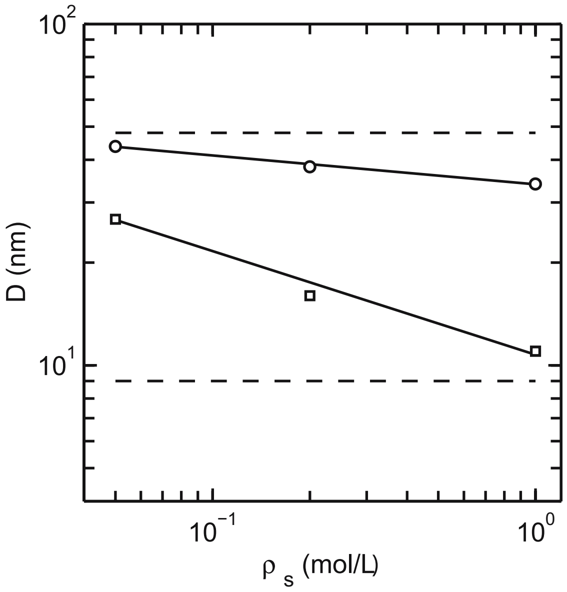

Fig. 13. The outer micelle D_{mic} (○) and crossover $2r_s$ (□) diameter versus the added salt concentration for fully ionized PS-*b*-PA ($DN = 1$) micelles [10]. The top dashed curve represents the micelle diameter without added salt, whereas the bottom dashed curve denotes the core diameter. The solid lines denote the scaling results for an osmotic polyelectrolyte star in the salt dominated regime with $D_{mic} \sim \rho_s^{-1/5}$ and $2r_s \sim \rho_s^{-1/2}$ for the outer and cross-over diameter, respectively. Notice the robustness of the outer micelle diameter against the addition of salt.

structure factor calculated with $\alpha = 4/3$ (100 and 50% charge) or 5/2 (10% charge). All fitted micelle diameters are displayed in Fig. 15. With added salt and/or at low degree of ionization, the coronal layers are less extended. The ionic strength and charge dependencies of the micelle diameter agree with the results obtained for more diluted samples discussed in the previous section. With increasing packing fraction, the diameter of the micelles decreases. However, the extent to which the coronal layers shrink is modest and similar under all circumstances. The gradual decrease in size is due to the restricted free volume, increased counterion adsorption, and/or Donnan salt partitioning between the coronal layer and the supporting medium.

9 Inter-Micelle Structure

Inter-micelle interference is more clearly demonstrated in Fig. 16, where the core structure factor has been divided by the core form factor (full charge and no added salt). Although the center of mass structure factor could also be derived from the corona structure factor, we have chosen to use the core structure

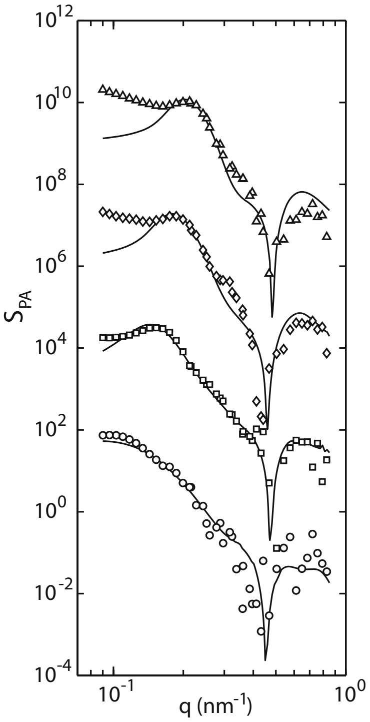

Fig. 14. Corona PA structure factor versus momentum transfer for fully charged PS-*b*-PA micelles without added salt [20]. The copolymer concentration is 44 (△), 30 (◇), 17 (□), and 4.4 (○) g/l from top to bottom. The data are shifted along the y-axis with an incremental multiplication factor. The curves represent the model calculations.

factor because the core form factor shows a smooth and moderate variation in the relevant q-range. The intensity of the correlation peaks first increases and eventually levels off with increasing packing fraction, which shows the progressive and saturating ordering of the micelles. Notice that for the present volume fractions the position of the primary peak is mainly determined by density, whereas the respective positions of the higher order correlation peaks are most sensitive to the value of the hard sphere diameter. The lines in Fig. 16 represent the hard sphere solution structure factor convoluted with the instrument resolution and fitted micelle densities ρ_{mic} and hard sphere diameters D_{hs}. The hard sphere model is capable of predicting the positions of the primary and higher order peaks. Furthermore, the ratio of the fitted micelle densities and known copolymer concentrations provides an alternative way to obtain the aggregation number. The average value of the aggregation number $N_{ag} = 98 \pm 10$, as obtained from the fitted densities, is in perfect agreement with the one obtained from the normalization of the structure factors. Clear

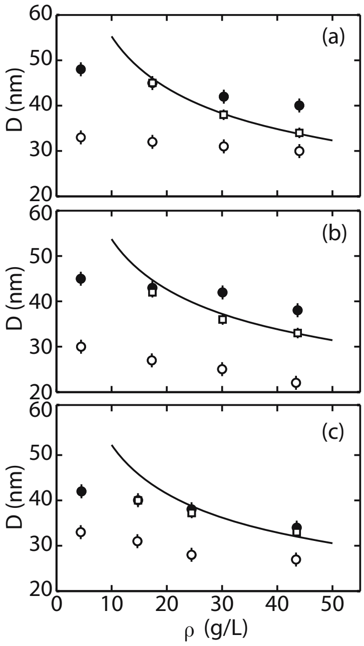

Fig. 15. Concentration dependence of the diameter of 100 (a), 50 (b), and 10% (c) charged PS-*b*-PA micelles: (●), D_{mic} without added salt; (◯), D_{mic} in 1.0 M (100 and 50%) or 0.04 M (10% charge) KBr [20]. The hard-sphere diameter of salt-free micelles D_{hs} is denoted by (□). The lines represent $\rho^{-1/3}$, i.e. the average inter-micelle distance.

deviations between the experimental data and the hard sphere prediction are observed in the low q-range for samples with higher micelle densities. Furthermore, the model underestimates the intensity of the second order peak with respect to the primary one. We have checked that a repulsive, screened Coulomb potential does not improve the fit, nor does it significantly influence the peak positions for reasonable values of the micelle charge [24]. The minor importance of the electrostatic interaction between the micelles and the relatively small net micelle charge due to the trapping of the counterions in the coronal layer are demonstrated by similar center of mass structure factors for 10, 50 and 100% charged micelles. The failure in predicting the relative amplitude of the higher order peak is probably related to the softness of the micelles; similar behavior has been reported for interpenetrating neutral polymer stars [36, 37]. The deviations observed in the low q-range might be due to long-range inhomogeneity in density, the formation of aggregates, and/or stickiness between the micelles. We have checked that the sticky hard sphere model does not improve the fit in the low momentum transfer range, but it gives a better description of the depth of the first minimum after the primary peak (result not shown) [25]. However, the derived distance of closest

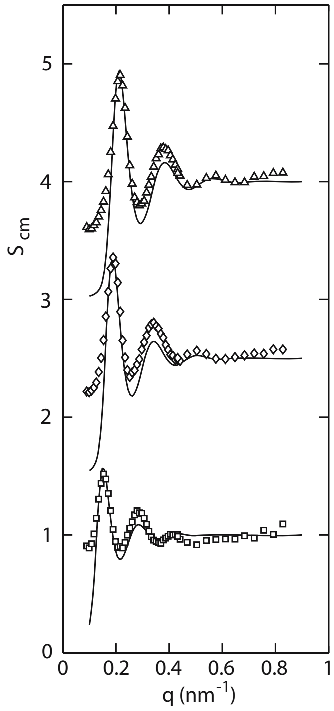

Fig. 16. Center of mass solution structure factor for fully charged PS-*b*-PA micelles versus momentum transfer [20]. The copolymer concentration is 44 (△), 30 (◇) and 17 (□) g/L from top to bottom. The data are shifted along the y-axis with an increment of 1.5 units. The curves represent the hard sphere solution structure factor.

micelle approach is the same as the hard sphere diameter and we have further refrained from interpreting our data with this more elaborate model.

The fitted outer micelle D_{mic} and hard sphere D_{hs} diameters as obtained from the corona form and solution structure factor analysis, respectively, are displayed in Fig. 15. D_{mic} and D_{hs} are estimated within a 3 and 2% accuracy margin, respectively, which is about the size of the symbols. The hard sphere diameters were derived for salt-free micelles only, because in the presence of excess salt inter-micelle interference is effectively suppressed. For the less concentrated, 15 and 17 g/l solutions, the hard sphere diameters equal the micelle diameters derived from the form factor analysis. This supports the applicability of the hard sphere interaction model in order to extract the effective hard sphere diameters. At higher packing fractions and for the 50 and 100% charged micelles in particular, the effective hard sphere diameters are significantly smaller than the outer micelle diameters. We take the difference as a measure of the extent to which the corona layers interpenetrate. Accordingly, the 100 and 50% charged, salt-free micelles interpenetrate around 17 g/l; for the smaller 10% charged micelles this happens at a higher concentration, say 25 g/l.

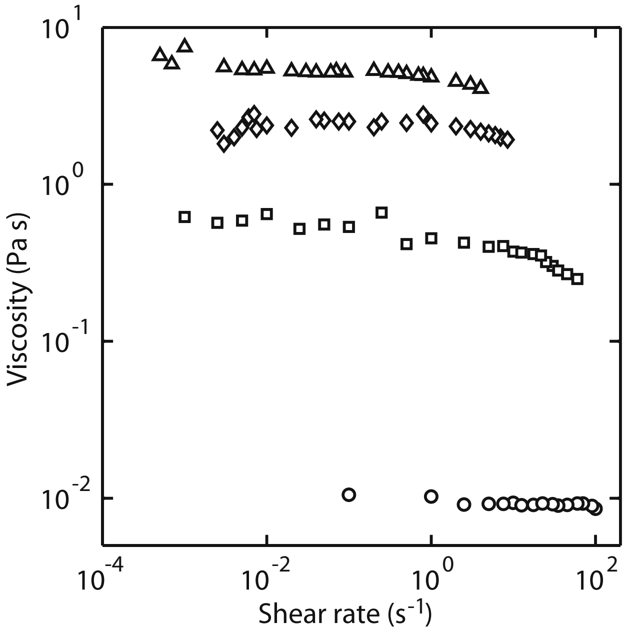

Fig. 17. Viscosity versus the shear rate for 50% charged PS-*b*-PA micelles without added salt [20]. The copolymer concentration is 44 (△), 30 (◇), 17 (□) and 4.5 (○) g/L from top to bottom. Reprinted with permission from [20]. Copyright (2005) American Institute of Physics.

Fig. 15 also displays the average distance between the micelles $\rho^{-1/3}$. Once the micelles interpenetrate, the effective hard sphere diameter equals $\rho^{-1/3}$. Based on the optimized micelle densities and hard sphere diameters, effective micelle volume fractions can be calculated. For interpenetrating micelles, the effective volume fraction is found to be constant within experimental accuracy and takes the value 0.53±0.02. Notice that, although this volume fraction corresponds with closely packed, simple cubic order, the center of mass structure factor remains liquid-like and no long-range order in the SAXS and SANS diffraction patterns is observed. Interpenetration of the arms of the micelle thus occurs when the effective volume fraction reaches the critical value 0.53 (and remains constant for higher micelle densities).

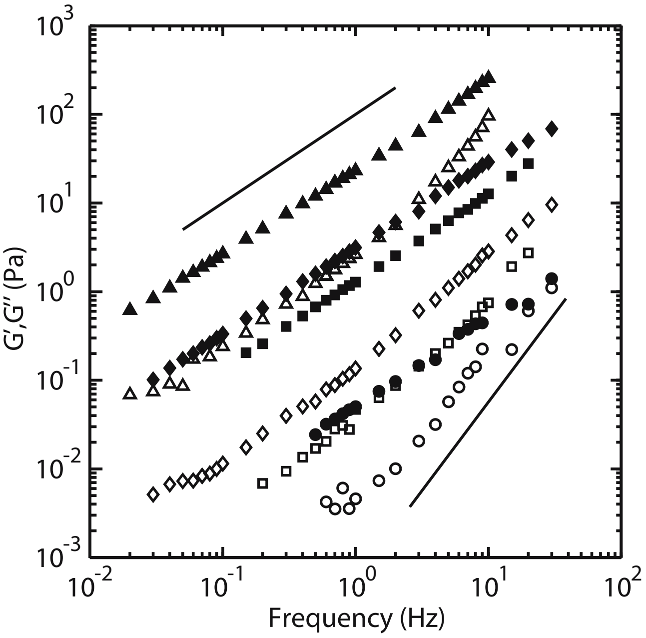

Fig. 18. Frequency dependence of storage G' (open symbols) and loss G" (filled symbols) modulus for 50% charged PS-b-PA micelles without added salt [20]. The copolymer concentration is 44 (△), 30 (◇), 17 (□), and 4.5 (○) g/L from top to bottom. The lines indicate ω^1 and ω^2 scaling. Reprinted with permission from [20]. Copyright (2005) American Institute of Physics.

10 Visco-Elastic Behavior

The interpenetration of the coronal layers has a profound influence on the visco-elastic properties [20]. All samples are fluid and flow when the test tubes are inverted. We have measured the viscosity of the solutions with 50% charged micelles. In excess salt (1 M KBr), the viscosity is in the range 1-2 mPa s, which is on the order of the viscosity of the solvent (data not shown). The viscosity versus shear rate of the samples without added salt is displayed in Fig. 17. A Newtonian plateau is observed, which increases in value by 3 orders of magnitude when the concentration is increased so that the coronal layers interpenetrate. Notice that the salt-free sample with the lowest micelle concentration has already a 10 fold higher viscosity than the ones with excess salt. For the more concentrated samples, the onset of shear thinning at high shear rates is also observed.

We have also measured the dynamic moduli of the solutions with 50% charged micelles without added salt. Data are shown in Fig. 18. For the lowest concentration, the dynamic moduli show viscous liquid behavior with $G'(\omega) \sim \omega^2$ and $G''(\omega) \sim \omega^1$. For interpenetrating micelles and in the lower frequency range in particular, $G'(\omega)$ and $G''(\omega)$ show approximately parallel scaling laws as a function of frequency with scaling exponents around unity. Such behavior has been observed for a wide variety of polymer gels and similar micellar solutions of polyelectrolytes with adhesive corona chains [2, 38]. Although we do not observe the transition to an elastic solid ($G' > G''$ and almost independent on frequency), an intuitive explanation of the parallel frequency scaling behavior of G' and G'' is the formation of an interconnected network of micelles by the interpenetration of the coronal layers as shown by the scattering experiments.

11 Conclusions and Outlook

Our PS-*b*-PA micelles have served as an excellent model system to investigate the properties of the spherical polyelectrolyte brush under various conditions. We have found that the effect of charge ordering in the coronal layer can be rationalized on the basis of scaling relations originally derived for osmotic polyelectrolyte stars. This is mainly due to the relatively large functionality of our micelles, which results in the confinement of small counterions in the coronal layer. Accordingly, the main stretching force of the coronal chains is due to the osmotic pressure exerted by the trapped counterions. Due to the osmotic stretching force, the polyelectrolyte corona chains take an (almost) fully stretched conformation at high charge and minimal screening conditions. Furthermore, the coronal layer is rather robust against the salinity generated by the presence of salt and against compression forces resulting from the interaction between brushes. With increasing packing fraction, the brushes eventually interdigitate which results in the formation of a physical gel and a dramatic increase in solution viscosity. These properties are important for the design of materials for technological applications as well as for our understanding of certain biological processes involving glycoprotein brushes such as synovial lubrication.

Owing to the high glass temperature of the core forming segments, our micelles have a fixed functionality and the spherical morphology does not change under the various conditions. Future work can focus on polyelectrolyte block copolymers with a liquid domain of the self-assembled hydrophobic attachment under true thermodynamic equilibrium conditions. Here, as an additional level of complexity, the morphology can be controlled by the chemical potentials of the constituents, which might depend on stimuli such as temperature, pH, and ionic strength. Furthermore, so far we have studied the simplest possible morphology, i.e. spherical micelles. An obvious extension of our work is to investigate the properties of other supra-molecular assemblies of polyelectrolyte diblock copolymers such as rods and vesicles. The rod-like assemblies are particularly promising, because the asymmetric shape might result in the formation of a lyotropic liquid crystal once the packing fraction exceeds a certain critical value. The vesicular structures have already proven to be of interest for, e.g., the encapsulation of clone vector DNA for gene delivery [39].

Acknowledgement. I thank Wendy Groenewegen, Sasha Korobko, Wim Jesse, Stefan Egelhaaf, and Alain Lapp for their collaboration. I acknowledge the Institute Laue-Langevin, Laboratoire Léon Brillouin, and the European Synchrotron Radiation Facility in providing the neutron and X-ray research facilities, respectively. The staff of these facilities is thanked for their assistance during the scattering experiments.

References

1. G. Riess, Prog. Polym. Sci. 28, 1107 (2003).
2. S. R. Bhatia, A. Mourchid, and M. Joanicot, Curr. Opin. Colloid Interface Sci. 6, 471 (2001).
3. A. Albersdörfer and E. Sackmann, Eur. Phys. J. B 10, 663 (1999).
4. M. Tanaka, F. Rehfeldt, M. F Schneider, G. Mathe, A. Albersdörfer, K. R Neumaier, O. Purrucker, and E. Sackmann, J. Phys.: Condens. Matter 17, S649 (2005).
5. L. Zhang and A. Eisenberg, Science 268, 1728 (1995).
6. M. Moffitt, K. Khougaz, and A. Eisenberg, Acc. Chem. Res. 29, 95 (1996).
7. N. S. Cameron, M. K. Corbierre, and A. Eisenberg, Can. J. Chem. 77, 1311 (1999).
8. P. Guenoun, F. Muller, M. Delsanti, L. Auvray, Y.J. Chen, J.W. Mays, and M. Tirrell, Phys. Rev. Letters 81, 3872 (1998).
9. S. Förster, N. Hermsdorf, C. Bottcher, and P. Lindner, Macromolecules 35, 4096 (2002).
10. J.R.C. van der Maarel. W. Groenewegen, S.U. Egelhaaf, and A. Lapp, Langmuir 16, 7510 (2000).
11. M. Daoud, and J.-P. Cotton, J. Phys. 43, 531 (1982).
12. W. D. Dozier, J. S. Huang, and L. J. Fetters, Macromolecules 24, 2810 (1991).
13. K. A. Cogan, A. P. Gast, and M. Capel, Macromolecules 24, 6512 (1991).
14. S. Förster, E. Wenz, and P. Lindner, Phys. Rev. Letters 77, 95 (1996).
15. C. M. Marques, D. Izzo, T. Charitat, and E. Mendes, Eur. Phys. J. B. 3, 353. (1998).
16. W. Groenewegen, S. U. Egelhaaf, A. Lapp, and J. R. C. van der Maarel, Macromolecules 33, 3283 (2000).
17. W. Groenewegen, A. Lapp, S. U. Egelhaaf, and J. R. C. van der Maarel, Macromolecules 33, 4080 (2000).
18. L. Belloni, M. Delsanti, P. Fontaine, F. Muller, P. Guenoun, J.W. Mays, P. Boesecke, and M. Alba, J. Chem. Phys. 119, 7560 (2003).
19. A. V. Korobko, W. Jesse, S. U. Egelhaaf, A. Lapp, and J. R. C. van der Maarel, Phys. Rev. Letters 93, 177801 (2004).
20. A. V. Korobko, W. Jesse, A. Lapp, S. U. Egelhaaf, and J. R. C. van der Maarel, J. Chem. Phys. 122, 024902 (2005).
21. Notice that this definition differs from the situation for homopolymers, where the monomer is usually considered the elementary scattering unit.
22. J. K. Percus and G. J. Yevick, Phys. Rev. 110, 1 (1958).

23. C. N. Likos, H. Lowen, M. Watzlawek, B. Abbas, O. Jucknischke, J. Allgaier, and D. Richter, Phys. Rev. Letters 80, 4450 (1998).
24. J. B. Hayter and J. Penfold, Mol. Phys. 42, 109 (1991).
25. R.J. Baxter, J. Chem. Phys. 49, 2770 (1968).
26. S. Förster and C. Burger, Macromolecules 31, 879 (1998).
27. L. Auvray, C. R. Acad. Sc. Paris 302, 859 (1986).
28. L. Auvray and P. G. de Gennes, Europhys. Letters 2, 647 (1986).
29. P. G. de Gennes, Scaling Concepts in Polymer Physics, Cornell University Press, Ithaca, 1979.
30. A. Yu. Grosberg and A. R. Khohklov, Statitical Physics of Macromolecules, American Institute of Physics Press, New York, 1994.
31. O. V. Borisov, J. Phys. II 6, 1 (1996).
32. O. V. Borisov and E. B. Zhulina, Eur. Phys. J. B 4, 205 (1998).
33. This value was obtained from the experimental pK = 7.2 of simple salt-free 0.014 mole of PA/dm3 PS-b-PA solutions, unpublished results.
34. M. Heinrich, M. Rawiso, J. G. Zilliox, P. Lesieur, J. P. Simon, Eur. Phys. J. E 4, 131 (2001).
35. J. R. C. van der Maarel, L. C. A. Groot, J. G. Hollander, W. Jesse, M. E. Kuil, J. C. Leyte, L. H. Leyte-Zuiderweg, M. Mandel, J. -P. Cotton, G. Jannink, A. Lapp, and B. Farago, Macromolecules 26, 7295 (1993).
36. A. Jusufi, C. N. Likos, and H. Löwen, Phys. Rev. Letters 88, 8301 (2002).
37. A. Jusufi, C. N. Likos, and H. Löwen, J. Chem. Phys. 116, 11011 (2002).
38. H. H. Winter and M. Mours, Adv. Polym. Sci. 134, 165 (1997).
39. A. V. Korobko, C. Backendorf, and J. R. C. van der Maarel, J. Phys. Chem. B 110, 14550 (2006).